J Neurophysiol 102: 2396–2409, 2009.
First published August 19, 2009; doi:10.1152/jn.00095.2009.

Dendritic Spine Remodeling After Spinal Cord Injury Alters Neuronal Signal Processing

Andrew M. Tan,* Jin-Sung Choi,* Stephen G. Waxman, and Bryan C. Hains
Departments of Neurology and Center for Neuroscience and Regeneration Research, Yale University School of Medicine, New Haven, and Rehabilitation Research Center, Veterans Affairs Connecticut Healthcare System, West Haven, Connecticut

Submitted 2 February 2009; accepted in final form 12 August 2009

Tan AM, Choi J-S, Waxman SG, Hains BC. Dendritic spine remodeling after spinal cord injury alters neuronal signal processing. *J Neurophysiol* 102: 2396–2409, 2009. First published August 19, 2009; doi:10.1152/jn.00095.2009. Central sensitization, a prolonged hyperexcitability of dorsal horn nociceptive neurons, is a major contributor to abnormal pain processing after spinal cord injury (SCI). Dendritic spines are micron-sized dendrite protrusions that can regulate the efficacy of synaptic transmission. Here we used a computational approach to study whether changes in dendritic spine shape, density, and distribution can individually, or in combination, adversely modify the input–output function of a postsynaptic neuron to create a hyperexcitable neuronal state. The results demonstrate that a conversion from thin-shaped to more mature, mushroom-shaped spine structures results in enhanced synaptic transmission and fidelity, improved frequency-following ability, and reduced inhibitory gating effectiveness. Increasing the density and redistributing spines toward the soma results in a greater probability of action potential activation. Our results demonstrate that changes in dendritic spine morphology, documented in previous studies on spinal cord injury, contribute to the generation of pain following SCI.

INTRODUCTION

Central sensitization, a mechanism thought to contribute to chronic neuropathic pain conditions, can result from either peripheral or central nervous system injury (Ji et al. 2003; Woolf 1994). Hyperexcitability of dorsal horn (DH) nociceptive neurons results from central sensitization and is associated with allodynia, a painful response to normally nonnoxious stimuli, and hyperalgesia, a heightened sensitivity to painful stimuli caused by pain-signal amplification within the CNS (Finnerup et al. 2001, 2003). The hyperexcitable state of DH neurons after injury is chronic and resilient, which suggests that injury-induced changes to pain-sensory signal processing within the nervous system reside in a firmly established pathological state. Processes that are known to contribute to DH hyperexcitability include: the loss of inhibitory GABAergic input (Drew et al. 2004), changes to postsynaptic receptors (Agrawal and Fehlings 1997; South et al. 2003), abnormal expression of sodium ion channels (Hains et al. 2003; Waxman and Hains 2006), and aberrant remodeling of afferent fibers and their branches (Romero et al. 2000; Woolf et al. 1992).

Localized increases in synaptic strength through the de novo formation and/or elaboration of postsynaptic dendritic spines constitute a structural basis for learning and memory in the CNS. Similar cellular mechanisms may also contribute to neuropathic pain after spinal cord injury (SCI) (Ji et al. 2003). Dendritic spines are micron-sized protrusions from dendrites that provide postsynaptic sites for presynaptic input. Dendritic spines are associated with highly convergent inputs, e.g., on pyramidal cells and neurons in the spinal cord DH (Svendsen et al. 1999; Yuste and Majewska 2001). Dendritic spines regulate the efficacy of synaptic transmission and can thereby alter the transmission of electrical information in sensory pathways (Bourne and Harris 2007; Calabrese et al. 2006). Changes in dendritic spine morphology after injury can thus alter the input–output function of neurons (Pongracz 1985; Segev and Rall 1988). Our previous data (Tan et al. 2008) and evidence in the literature as described in the following text indicate that dendritic spine morphology can change following an activity-dependent event and after disease and injury. *1*) Dendritic spines can elaborate from a thin, filopodia-like structure to a mushroom shape, a structure associated with increased synaptic efficacy and fidelity (Bourne and Harris 2007; Yuste and Majewska 2001); *2*) the density of spines can increase along the dendrite, providing more sites for postsynaptic connections (Bonhoeffer and Yuste 2002; Yuste and Bonhoeffer 2001); and *3*) spines can redistribute along the dendrite (Kim et al. 2006; Ruiz-Marcos and Valverde 1969). It is not yet known whether dendritic spine remodeling can contribute to the hyperexcitable state of nociceptive dorsal horn neurons associated with neuropathic pain after SCI.

Here we asked whether changes in dendritic spine morphology can contribute to the neuronal hyperexcitability associated with neuropathic pain. To address this question we used the NEURON simulation environment to model the effects of dendritic spine shape, distribution, and density on the transduction of signals onto a postsynaptic neuron. The results demonstrate that a switch from thin spines to a mushroom spine shape, as observed in DH neurons after SCI (Tan et al. 2008), produces alterations in the synaptic potential waveform and input–output functions that can contribute to neuronal hyperexcitability. A simultaneous increase in spine density and distribution of spines closer to the soma, which are also observed in DH neurons after SCI (Tan et al. 2008), produce an amplification of excitatory postsynaptic input. These results suggest *1*) a new mechanism that contributes to neuropathic pain and *2*) that methods that disrupt injury-induced changes in dendritic spine morphology may provide a new therapeutic approach to pain following SCI.

* These authors contributed equally to this work.

Address for reprint requests and other correspondence: S. G. Waxman, Center for Neuroscience and Regeneration Research, VA CT Healthcare System (127A), 950 Campbell Avenue, Bldg. 34, West Haven, CT 06516 (E-mail: stephen.waxman@yale.edu).

METHODS

Spinal cord injury

In vivo experiments were performed in accordance with National Institutes of Health guidelines for the care and use of laboratory animals and were approved by the Yale University Institutional Animal Use Committee. Adult male Sprague–Dawley rats (175–200 g) were anesthetized with a mixture of ketamine and xylazine (80/5 mg/kg, administered intraperitoneally) and subjected to spinal cord contusion injury. Briefly, the NYU/MASCIS impact injury device (Gruner 1992) was used to produce SCI at spinal segment T9 (Hains and Waxman 2006). Following laminectomy, a 2.0-mm-diameter rod (10 g) was dropped from a 25-mm height onto the exposed spinal cord. Sham control animals underwent laminectomy only. Postoperative treatments included twice-daily subcutaneous injections of 0.9% saline solution for rehydration (2.0 ml) and Baytril (0.3 ml, 22.7 mg/ml) to prevent bladder infection. Bladders were manually expressed twice daily until reflex bladder function returned, usually within 10 days after injury. Animals were housed under a 12-h light/dark cycle in a pathogen-free area with water and food given without restriction.

Histology

Intact and SCI rats were killed 31 days postsurgery for Golgi–Cox staining using an FD Rapid GolgiStain Kit (FD Neurotechnologies, Ellicott, MD). Fresh unfixed spinal cord tissue was removed, washed in distilled water, and immersed in the impregnation solutions (FD Neurotechnologies). Following a series of steps according to the manufacturer's instructions, 200-μm-thick tissue sections were cut on a vibratome and mounted on gelatinized glass slides. Sections were stained, rinsed twice in distilled water, dehydrated, cleared, and coverslipped. Five criteria were used to sample and analyze whole cells with morphology similar to that observed for wide-dynamic range (WDR) neurons identified by Woolf (1987): *1*) neurons were located within laminae IV and V; *2*) Golgi-stained neurons must have had dendrites and spines that were completely impregnated, appearing as a continuous length; *3*) at least one dendrite extended into an adjacent lamina relative to the origin of the cell body; *4*) at least half of the primary dendritic branches remained within the thickness of the tissue section, such that their endings were not cut and instead appeared to taper into an ending; and *5*) the cell body diameter was 20–50 μm. Images similar to those shown in Fig. 1 were captured with a Nikon Eclipse E800 microscope with a HQ Coolsnap camera (Roper Scientific, Tucson, AZ).

Membrane and ionic mechanisms

The modeling parameters we used have been described previously (Miller et al. 1985; Rusakov et al. 1996; Wilson 1984). Passive membrane resistivity was: $R_m = 10\ k\Omega\cdot cm^2$; capacitance was: $C_m = 1.0\ \mu F/cm^2$; cytoplasmic resistivity in the soma and dendrites was: $R_a = 100\ \Omega\cdot cm$, and $R_a = 200\ \Omega\cdot cm$, respectively, in dendritic spines to account for dense "packing" of organelles such as the spine apparatus. Somatic active membranes incorporated Hodgkin–Huxley (H-H) channels (Hodgkin and Huxley 1952) with parameters: sodium conductance, $g_{NA} = 0.12\ S/cm^2$; potassium conductance, $g_K = 0.036\ S/cm^2$; and passive leak conductance, $g_L = 0.3\ mS/cm^2$, as provided in NEURON. Dendritic spine head active membranes contained H-H channel densities set at 10-fold (10·H-H) that in the soma. H-H channel models have been used in previous computational studies with similar ion channel densities, membrane resistances, and capacitance (Lopez-Aguado et al. 2002; Rusakov et al. 1996; Segev and Rall 1988, 1998). The only variable parameter was geometry. All other parameters remained numerically constant in our model. Because these active and passive membrane parameters were held constant, the qualitative results reported here are dependent on the geometry of the dendritic branch, spines, and soma, rather than on changes in ionic mechanisms or passive membrane properties.

Modeling synaptic input

An α-function was used to simulate synaptic conductance. This integrated modeling tool in NEURON for simulating postsynaptic

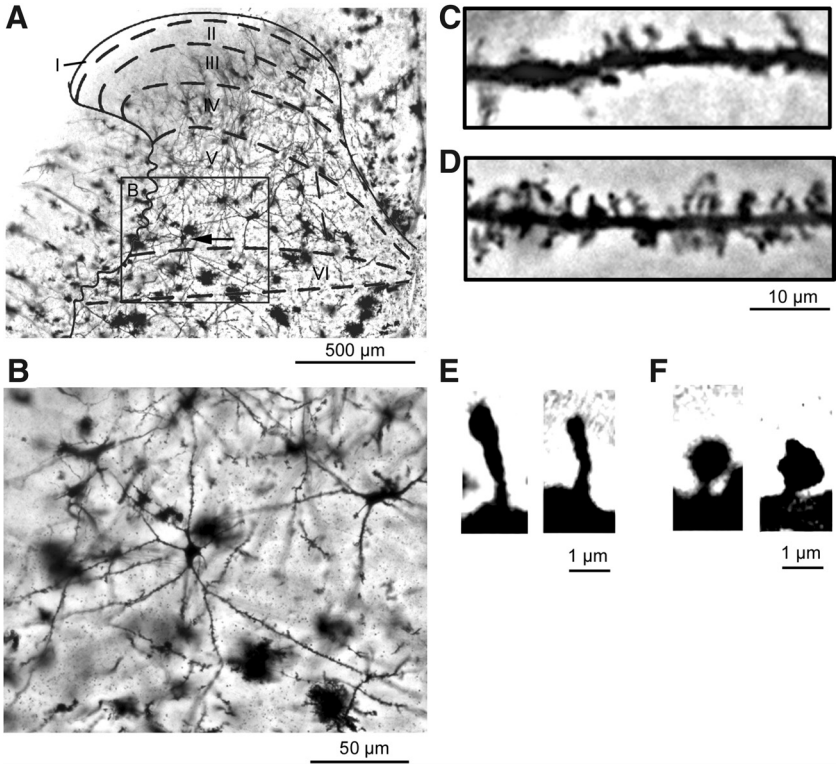

FIG. 1. Coronal sections of spinal cord tissue from the lumbar enlargement were Golgi-stained and examined for dendritic spines. *A*: a sample neuron located in dorsal horn (DH) lamina 5 (black arrow). *B*: magnified view of neuron shown in *A* (see *inset*). *C*: a dendritic segment from an intact animal. *D*: after spinal cord injury (SCI), there is an increase in spine density. *E*: high-power image of 2 sample thin-shaped spines. *F*: mushroom spines appear with enlarged, bulblike head structures.

input conductances is based on an approximation of actual postsynaptic potential waveforms obtained from electrophysiological recordings rather than the underlying electrochemical mechanisms. The α-function, however, can be used to approximate most synaptic currents with a small number of parameters and provides a widely used model for computing postsynaptic current (Destexhe et al. 1994; Rall et al. 1967). The synaptic current (I) generated by the α-function is as follows

$$I = g_{max}(t/\tau_{input}) \exp(-t/\tau_{input})(V - E) \quad (1)$$

where t is the time of synaptic activation; τ_{input} is a time constant of synaptic conductance, which is equal to the time when input transient reaches its peak conductance (g_{max}); and E is the reversal potential of neurotransmitter evoked synaptic current. For voltage-independent α-amino-3-hydroxy-5-methyl-4-isoxazoleproprionate (AMPA)–type excitatory current, the time to peak was set (Frank and Fuortes 1956; Pongracz 1985), where τ_{input} = 0.2 ms and maximum conductance (g_{max}) was varied throughout the experiments (Wilson 1984). The reversal potential on reaching maximum conductance was set to E = 0 mV. For γ-aminobutyric acid (GABA)–type inhibitory current, the time to peak was set at τ_{input} = 7 ms for Fig. 11 because of lack of effect on excitability with shorter τ_{input}, and maximum conductance (g_{max}) was varied between 50 and 1,000 nS. GABA synaptic currents had a reversal potential of −75 mV. For the purpose of examining the effects on waveform shape produced through varying the time to maximum conductance we set τ_{input} = 0.05, 0.2, 0.5, 1, 3, 5, and 7 ms for both excitatory and inhibitory synaptic models (Figs. 2 through 5).

Preliminary simulation experiments showed that mushroom spines had faster and larger postsynaptic responses compared with those of thin spines. To clarify the time constant of the dendritic spine itself (τ_{spine}), we used a step depolarization to model presynaptic input, as opposed to an α-function (see Supplemental Fig. S1).[1] Briefly, we applied a step depolarization (V_{hold} = −70 mV, V_{test} = 0 mV) on all spine models and fit the resultant output (Supplemental Fig. S1, *B–E*) with a monoexponential function to obtain τ_{spine} (Supplemental Fig. S1*F*). Thus we defined the spine time constant as the monoexponential change of membrane potential at the base of the dendritic spine in response to the delivery of a step depolarization (from −70 to 0 mV) at the spine head. The resultant output, however, from most of the spine models did not fit well with a monoexponential function (see Supplemental Fig. S1*F*) or even with a biexponential function for some spine models. The τ_{spine} in all models was >0.1 ms, suggesting that τ_{spine} might have been slower than the fastest τ_{input}. However, the resultant output produced by a τ_{input} of 0.05 ms (red line, Supplemental Fig. S1, *B–E*) was always slower than that produced by the step depolarization (black line, Supplemental Fig. S1, *B–E*), indicating that simulations even with τ_{input} of 0.05 ms, which is faster than τ_{spine}, produced interpretable results.

Modeling dendritic spines

Dimensional information about dendritic spines located on dorsal horn neurons is available from our previous report (Tan et al. 2008) and we used spine geometries that fell within these published ranges to derive parameters for the spine neck, spine head, and spine volume (Calabrese et al. 2006; Galofre et al. 1987; Garcia-Lopez et al. 2006; Harris and Kater 1994; Kim et al. 2006). To construct spines and examine the effects of spine shape on the signal transduction onto the parent dendritic branch, we used a two-compartment model: spine neck and head. To consider the effects of geometric changes only (Segev and Rall 1998), we modeled spine shapes based on two different assumptions for underlying spine shape change (see RESULTS). For the first assumption (#1: dendritic spines mature in shape by the addition of cellular material) we modeled three spines each having the same neck dimensions [neck diameter (d_n) = 0.5 μm, neck length (l_n) = 0.5 μm] while varying the size of the spine head: small (1x), head diameter (d_h) = 0.5 μm, head length (l_h) = 0.5 μm; medium (2x), d_h = 1.0 μm, l_h = 1.0 μm; large (3x), d_h = 1.5 μm, l_h = 1.5 μm. These three sets of parameters produced thin, intermediate, and mushroom-shaped spines, respectively (see Figs. 3 and 4, *A*, *B*, and *C*). We also modeled spines based on a second assumption (#2: dendritic spines change shape via local cytoskeletal rearrangement and independent of the addition of cellular material). Here all spines were modeled with similar volume, reflecting a conservation of cytoplasmic mass, while varying the dimensions of the spine neck and head: thin spine shape, d_n = 0.5 μm, l_n = 3.0 μm, d_h = 0.5 μm, l_h = 0.5 μm; intermediate spine shape, d_n = 0.5 μm, l_n = 1.85 μm, d_h = 0.75 μm, l_h = 0.75 μm; mushroom spine shape, d_n = 0.5 μm, l_n = 0.5 μm, d_h = 1.0 μm, l_h = 0.75 μm (see Figs. 5 and 6, *A*, *B*, and *C*). Presynaptic α-function stimuli were directed on the spine head. The resultant postsynaptic responses were recorded at the base of the spine neck and in the soma.

For all further simulation experiments (see Figs. 7–12), we used the second assumption to model spine-shape variations (i.e., the volume-constant condition). We favored the use of this model based on literature that demonstrates localized cytoskeletal rearrangement within dendritic spines during synaptic plasticity events (Calabrese et al. 2006; Carlisle and Kennedy 2005; Chen et al. 2007; Chetkovich et al. 2002; Halpain 2006; Matsuzaki et al. 2004). In addition, we found that preliminary quantitative data demonstrated that spines modeled following the second assumption produced the greatest differences in the transduced synaptic potential across spine geometrical variations. We therefore used these spine shapes in the neuronal input–output experiments. To compare the effect of dendritic spine geometry on simulated excitatory and inhibitory postsynaptic potential (EPSP and IPSP, respectively) waveforms, we used four quantitative indices: *1*) peak amplitude of the synaptic potential; *2*) latency from stimulation-to-peak; *3*) width of the waveform at half-peak amplitude, which is a useful measure of the sharpness of the waveform; and *4*) area under the waveform curve, which provides a measure of the overall impact of a synaptic potential (Rall 1967).

Simplified neuron morphology

To investigate how dendritic spines affect the input–output function of neurons, we constructed a simplified neuron using cylindrical compartments as building blocks, as performed previously (Wilson 1984). Although neurons in the dorsal horn have dendritic branches with secondary projections (see Fig. 1*B*), we simplified this complexity with assumptions described by Rall (1967), which have been supported in other relevant computational models (Pongracz 1985). Briefly, the computational rationale for the simplification of complex neuronal structure used in our study is based on an insightful concept: geometric nonuniformity within the "real" neuron can be represented by separate compartments within the model, each containing appropriate simulation parameters (Rall et al. 1967). Therefore if biophysical and geometric variables are the same for the soma and dendritic branch, then differences in the quantitative indices of the synaptic potentials should be attributable to changes in spine morphology. Previous studies have demonstrated that information gathered from these simple neuronal models can be used to complement and interpret experimental data, providing insight into the mechanisms underlying the synaptic transmission process (Segev and Rall 1988, 1998). The basic framework of our neuronal model contained a soma [spherical shape defined as: diameter (d) = 30 μm; length (l) = 30 μm] and single dendritic branch (d = 2 μm; l = varied). This model appears as a "ball-and-stick" (see Figs. 7–12) (Pongracz 1985). We then attached one or more dendritic spines, varying in shape, onto the dendritic branch at predefined distances from the soma. Depending on the simulation experiment, we placed recording electrodes at the soma and the base of the spine neck to measure the effects of dendritic spine

[1] The online version of this article contains supplemental data.

transformation of postsynaptic potentials. We simulated input without the addition of stochastic noise because the degree of synaptic convergence or divergence between the presynaptic neuron and the postsynaptic neuron is unknown. Dendritic spines were subjected to either a single stimulus or a stimulus train.

To examine the cumulative effects of spine density and spine distribution on the output of a postsynaptic neuron (see Fig. 12) the dendritic branch of the simple neuron was divided into nine compartments, each of the same length and diameter ($d = 2$ μm; $l = 50$ μm). The compartments closest and farthest from the soma contained no spines. This follows previous quantitative morphological studies on dorsal horn neurons that show no or few spines close to the soma, increased spine density in medial portions of the branch, and decreased spine density at distal regions (Garcia-Lopez et al. 2006; Ruiz-Marcos and Valverde 1969; Valverde and Ruiz-Marcos 1969). The spine density/distribution on the dendritic branch of the simplified neuron in the intact model used a total of six spines distributed at equally spaced intervals across a 350-μm length of the dendrite. For the SCI neuronal model, nine spines were distributed along the same length of dendrite. The first two dendritic length compartments contained twice the spine density compared with the intact neuron to correspond with the relative spine distribution obtained from previous anatomical data (Tan et al. 2008). All dendritic spines modeled here used the parameters of the thin spines shown in Figs. 5*A* and 6*A*. To execute the simulation, we stimulated all spines simultaneously and recorded the resultant activity from the soma. To test the effects of spine development into the mushroom-shaped structures on the input–output function of the neuron, we replaced five of nine spines in the SCI model with the mushroom-shaped spines shown in Figs. 5*C* and 6*C*. We chose this proportion because previous data (Tan et al. 2008) suggest that there is a nearly 50% postinjury increase in the density of mushroom spines, compared with that in preinjury conditions, and these spines are distributed closer to the soma. For repetitive stimulation, all spines were stimulated with a train of stimuli separated by 14-ms intervals (71.4 Hz) (see RESULTS, Fig. 12*E*).

RESULTS

Modeling has demonstrated that the unique structure and molecular composition of dendritic spines contribute to their ability to act as discrete isolated computational units (Pongracz 1985; Rall et al. 1967), filter electrical noise (Tsay and Yuste 2002, 2004), and aid in linear summation (Araya et al. 2006; Lev-Tov et al. 1983; Yuste and Urban 2004). Computational studies have also been used extensively to complement recent experimental data (Matsuzaki 2007; Matsuzaki et al. 2004; Segev and Rall 1998). Although in vivo studies have partially revealed the effects of dendritic spine changes on synaptic transmission, these studies were done on neurons outside the DH, e.g., in the hippocampus (Gazzaley et al. 2002; Halpain 2006). Because these cortical neurons have a pyramidal structure with an invariant orientation and project through specific anatomical lamina in a predictable trajectory, multiple electrodes can be used to stimulate and record at different locations on the same neuron. This is not the case for multireceptive dorsal horn neurons, which are found at widely varying locations, typically in dorsal horn laminae IV and V (Fig. 1*A*). These neurons do not project dendrites with predictable trajectories (Fig. 1*B*). Thus to perform our studies, we used the NEURON software package (see METHODS) designed for building models of individual neurons and networks.

Synaptic input mechanisms

To simplify modeling this biological process, we used an α-function. For synapses impinging directly on the dendrite, this α-function produced a skewed curve (measured at the stimulation site) (Fig. 2, *A* and *B*). These curves represent the electrical potential caused by the release of neurotransmitter, binding of postsynaptic receptors, and subsequent membrane depolarization or hyperpolarization. Changing the τ_{input} altered the shape of the synaptic potential recorded in the dendrite. An incremental increase in the τ_{input} from 0.05 to 7 ms resulted in a broadening of the depolarization (Fig. 2*A*) and hyperpolarization waveform (Fig. 2*B*). For inhibitory α-synapses, the peak amplitude reached a plateau at $\tau_{input} > 3$ ms to about 3.2

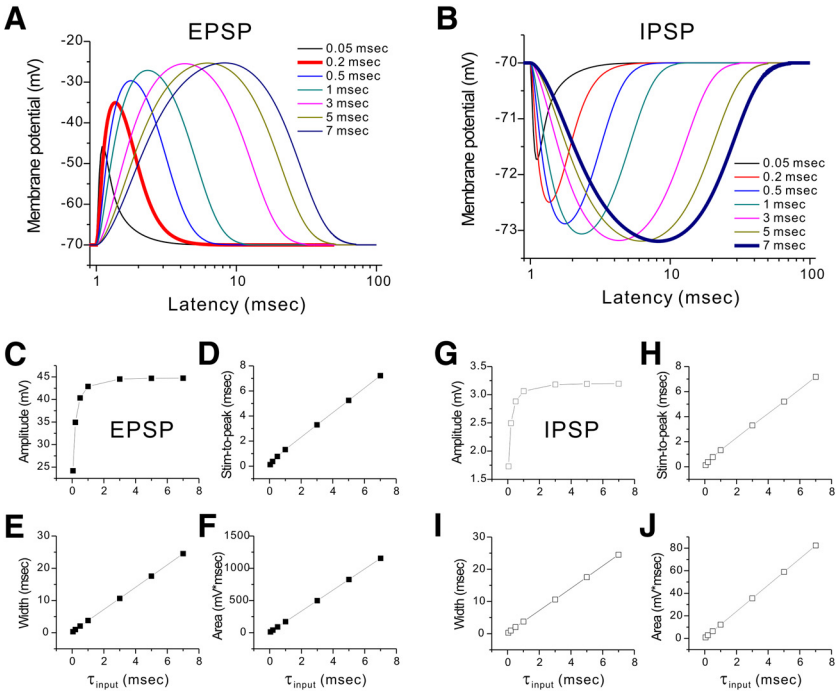

FIG. 2. Presynaptic input was modeled using an α-function. Synaptic conductances were placed on a 2-μm-diameter dendritic branch (cylinder shape) of infinite length. Recording of synaptic potentials were performed at the same location of the stimulation. *A*: graph representing an excitatory synaptic response with time to maximum conductance (τ_{input}) from 0.05 to 7 ms. An AMPA-like synapse is represented by the thick red line. *B*: graph representing an inhibitory synaptic response with τ_{input}. A GABA-like synapse is represented by the thick blue line. Peak amplitude (*C*, *G*), time-to-peak (*D*, *H*), width at 50% of peak (*E*, *I*), and area under curve (*F*, *J*) are analyzed from the EPSP (*A*) and IPSP (*B*) curves produced by the α-function synaptic conductance with $\tau_{input} = 0.05$, 0.2, 0.5, 1, 3, 5, and 7 ms. AMPA, α-amino-3-hydroxy-5-methyl-4-isoxazolepropionic acid; GABA, γ-aminobutyric acid; EPSP, excitatory postsynaptic potential; IPSP, inhibitory postsynaptic potential.

mV because of the small driving force between the reversal potential of the inhibitory conductance and resting membrane potential. For excitatory inputs, peak amplitude increased from 24.2 to 44.2 mV as the τ_{input} increased from 0.05 to 3 ms. Prolonging the τ_{input} over 3 ms has a relatively small effect on the synaptic potential amplitude. Other quantitative indices increased in an approximately linear fashion (Fig. 2, *D–F* and *H–J*). The latency for stimulation-to-peak and the duration at half-maximal amplitude increased proportionally for both excitatory and inhibitory inputs. The area under the curve also increased, illustrating the increased impact of the synaptic potential on the postsynaptic neuron.

Dendritic spine volume and shape modify signal transduction and synaptic potentials within the dendritic branch

We modeled spine geometries that fell within previously reported values for other types of neurons and our observations in the DH (Tan et al. 2008). To examine the effects of spine shape on signal transduction onto the parent dendritic branch, we used a two-compartment model. We divided the spine into two compartments—a head and a neck structure—assigning each compartment distinct parameters. The spine head contained voltage-gated ion channels with Hodgkin–Huxley (H-H) kinetics attached to a spine neck with passive membrane properties (Hodgkin and Huxley 1952). Each compartment was computed as a cylinder with a specific length and diameter. EPSPs and IPSPs were recorded from the base of spine neck in response to a single presynaptic stimulus onto the spine head (given as an α-function; see Fig. 2, *A* and *B*). We had considered two assumptions in spine-shape development: *1*) dendritic spines can mature by the addition of cellular material synthesized within the spine itself or transported from a location within the neuron but outside the spine (i.e., material transported from the soma) and inserted into the spine and *2*) the filamentous-actin cytoskeleton of each dendritic spine is rearranged locally and discretely without the addition of new cellular material (Calabrese et al. 2006; Carlisle and Kennedy 2005; Park et al. 2006; Wiens et al. 2005).

We first modeled the concept that spines may exist as a thin (Fig. 3*A*), intermediate (Fig. 3*B*), or mushroom-shaped structure (Fig. 3*C*). These spines have necks with similar volume, whereas the head compartment dimension varied as it is known to do under activity-dependent conditions (Carlisle and Kennedy 2005; Chen et al. 2007; Collin et al. 1997; Desmond and Levy 1988). When excitatory inputs were placed on thin (Fig. 3*A*) and intermediate spines (Fig. 3*B*), the resultant EPSP was attenuated, compared with inputs placed directly on the dendrite (see Fig. 1, *A* and *B*). The amplitude for the thin spine was smaller than that for intermediate and mushroom spines (Fig. 3*G*). Spine modulation of peak amplitude was input duration dependent, since increasing the time to maximum conductance from 0.05 to 7 ms initially increased and finally decreased EPSP peak amplitude for all spine shapes. This is shown clearly in Fig. 3*G*. In mushroom-shaped spines, the postsynaptic potential had a sharp up-slope waveform with the fastest rise times (Fig. 3*H*). The mushroom spine also had the narrowest synaptic potential demonstrated by the shortest duration at half-maximal amplitude of all spine shapes (Fig. 3*I*). As the time constant increased from 0.05 to 7 ms, the EPSP area for all spine shapes increased (Fig. 3*J*). The synaptic potential waveform transduced through the intermediate spine shape (Fig. 3, *G–J*) had quantitative indices that generally fell between thin and mushroom spines.

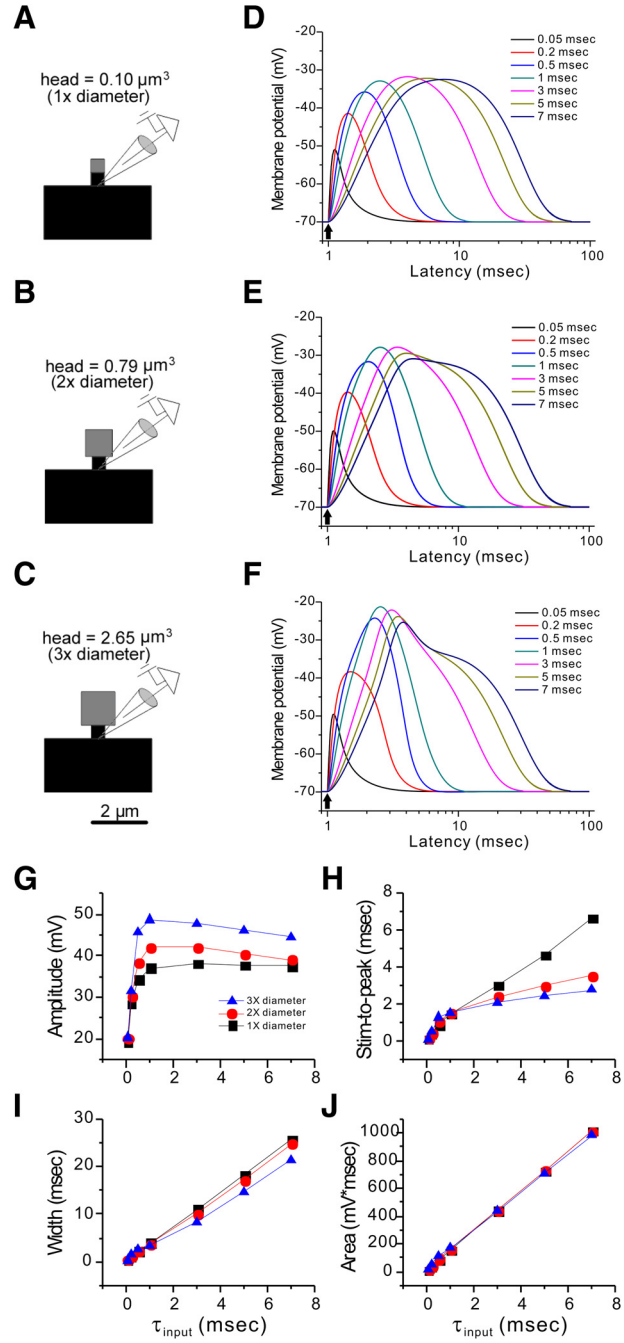

FIG. 3. Dendritic spine shapes were modeled based on the assumption that shape maturation occurs through the addition of cellular material into the spine head. A 2-compartment rationale was used to model spines with a neck and a head structure. The spine neck contained passive membrane properties. The spine head (gray region) contained Hodgkin–Huxley (1967) active membrane properties. Head size increased sequentially from a diameter of (*A*) 0.5 μm (1*x*) for small spines, (*B*) 1.0 μm (2*x*) for medium spines, and (*C*) 1.5 μm (3*x*) for large spines. Spines received excitatory synaptic conductance inputs on their head structure. Stimulation = black arrow. The resulting waveforms were graphed for (*D*) small spines, (*E*) medium spines, and (*F*) large spines. Graphs showing quantitative indices, such as peak amplitude (*G*), time-to-peak (*H*), width at 50% of peak (*I*), and area under curve (*J*), used to describe the EPSP for small, medium, and large spines, respectively.

The effects of spine shape on IPSPs (Fig. 4) were not as pronounced as those for EPSPs (see METHODS). The difference in amplitude between thin spines (Fig. 4*A*) and mushroom-shaped spines (Fig. 4*C*) was 0.19 mV and the difference between intermediate spines (Fig. 4*B*) and mushroom-shaped spines was 0.06 mV (Fig. 4*G*). The time for stimulation-to-peak was similar across spines for each incremental increase in τ_{input}. On stimulation, the intermediate spine shape produced an IPSP waveform with characteristics close to those of thin spines. The mushroom spine had a 5 to 11% increase (for τ_{input} of 7 and 0.05 ms, respectively) in synaptic potential area compared with that of thin spines, demonstrating that the overall impact of an IPSP increases with increasing spine head size the same as the EPSP. In contrast, mushroom spines had a 2 to 7% decrease (for τ_{input} of 7 and 0.05 ms, respectively) in synaptic potential width compared with that in thin spines, illustrating a narrowing of the IPSP waveform with increasing spine head size.

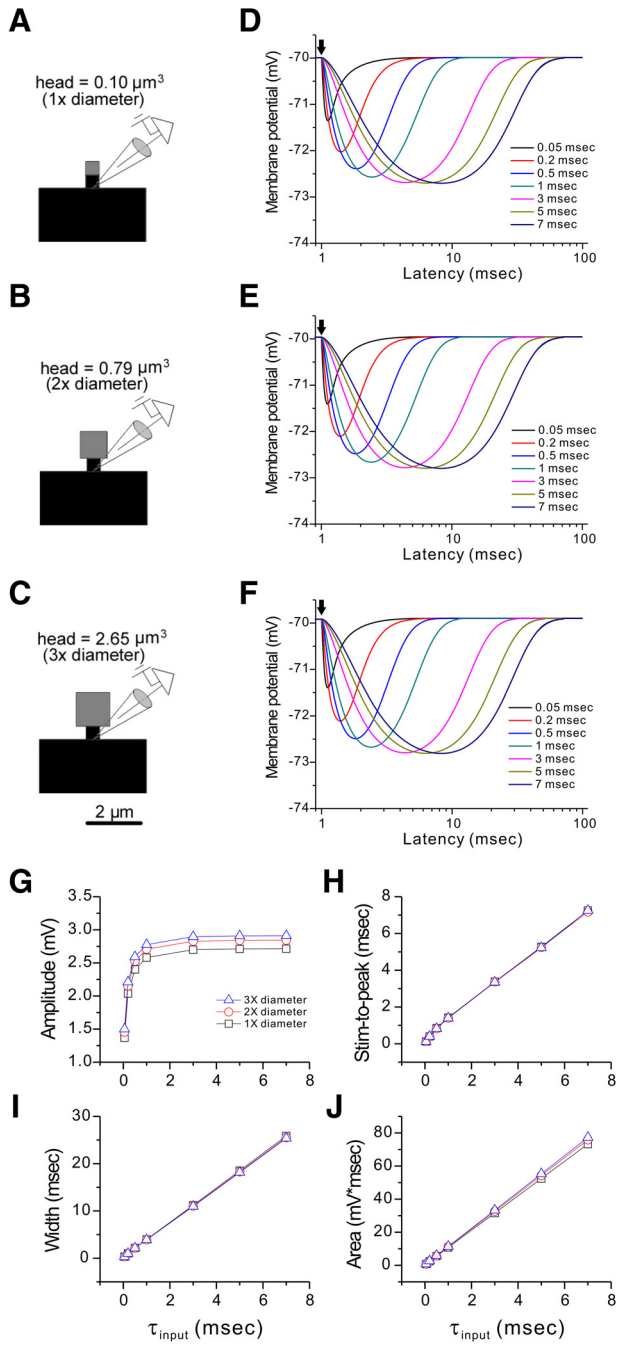

FIG. 4. Dendritic spine shapes were modeled similar to the previous figure. Head size increased sequentially from a diameter of (*A*) 0.5 μm for small spines, (*B*) 1.0 μm for midium spines, and (*C*) 1.5 μm for large spines. Spines received inhibitory synaptic conductance inputs on their head structure. Stimulation = black arrow. The resulting waveforms were graphed for (*D*) small spines, (*E*) medium spines, and (*F*) large spines. Graphs showing quantitative indices, such as peak amplitude (*G*), time-to-peak (*H*), width at 50% of peak (*I*), and area under curve (*J*), used to describe the IPSP for small, medium, and large spines, respectively.

We also constructed spine shapes based on the second assumption that spine geometrical parameters change from intrinsic, local cytoskeletal rearrangement. This may occur through molecular mechanisms that regulate filamentous-actin such as Rac- and Rho-GTPase activity (Bonhoeffer and Yuste 2002; Nakayama et al. 2000; Tashiro and Yuste 2004; Tashiro et al. 2000). Here spines were constructed such that their total volume remained constant, whereas the volumetric ratio of the spine head and neck varied (Fig. 5, *A–C*). As these ratios shifted toward the larger spine head, the synaptic potential increased in amplitude (Fig. 5*G*), the EPSP waveform sharpened (Fig. 5*I*), and the EPSP area increased (Fig. 5*J*). This resulted in the mushroom spine (Fig. 5, *C* and *F*) producing the greatest amplitude and narrowest EPSP waveform on receiving presynaptic input. In contrast, thin spines had the lowest amplitude, the broadest waveform shape, the longest latency from stimulation-to-peak amplitude, and the smallest EPSP area (Fig. 5, *D* and *G–J*). Quantitative indices changed similarly for inhibitory inputs (Fig. 6). IPSP amplitude and area increased with increasing head size. In addition, the IPSP width decreased with increasing head size. Together, these results demonstrate that a change in spine shape from a thin to a mushroom-shaped structure potentiates the signal transmitted on the dendritic branch while narrowing the waveform, which could contribute to maintaining the discretization of an electrical signal. All of the following simulation experiments used the second assumption (i.e., volume-constant condition) to model spine geometry.

Effect of dendritic spine location

To examine the effects of spine location on the dendritic branch, a thin or mushroom spine was placed at 10-μm intervals between 10 and 100 μm from the soma (Fig. 7*A*). To exclude the possibility of activating an action potential, the soma contained only passive membrane properties. An AMPA-like excitatory presynaptic input (τ_{input} = 0.2 ms, g_{max} = 50 nS) was placed on the spine and the resultant EPSP passively propagated along the branch was recorded in the soma (Fig. 7, *D* and *E*). As expected, increasing the distance of the spine from the soma decreased the amplitude and broadened the EPSP transmitted through both spine shapes. The EPSP produced through the mushroom spine (Fig. 7*E*) had a narrower width compared with that of the thin spine (Fig. 7*D*), demonstrating a sharper waveform. As the distance from the soma increased from 10 to 100 μm, the peak amplitude of the EPSP decreased at a greater rate for the mushroom spine than that for the thin spine: up to a 60 and 57% decrease for the thin and mushroom spines, respectively (Fig. 7*F*). In addition, the EPSP width increased at a greater rate for potentials transduced

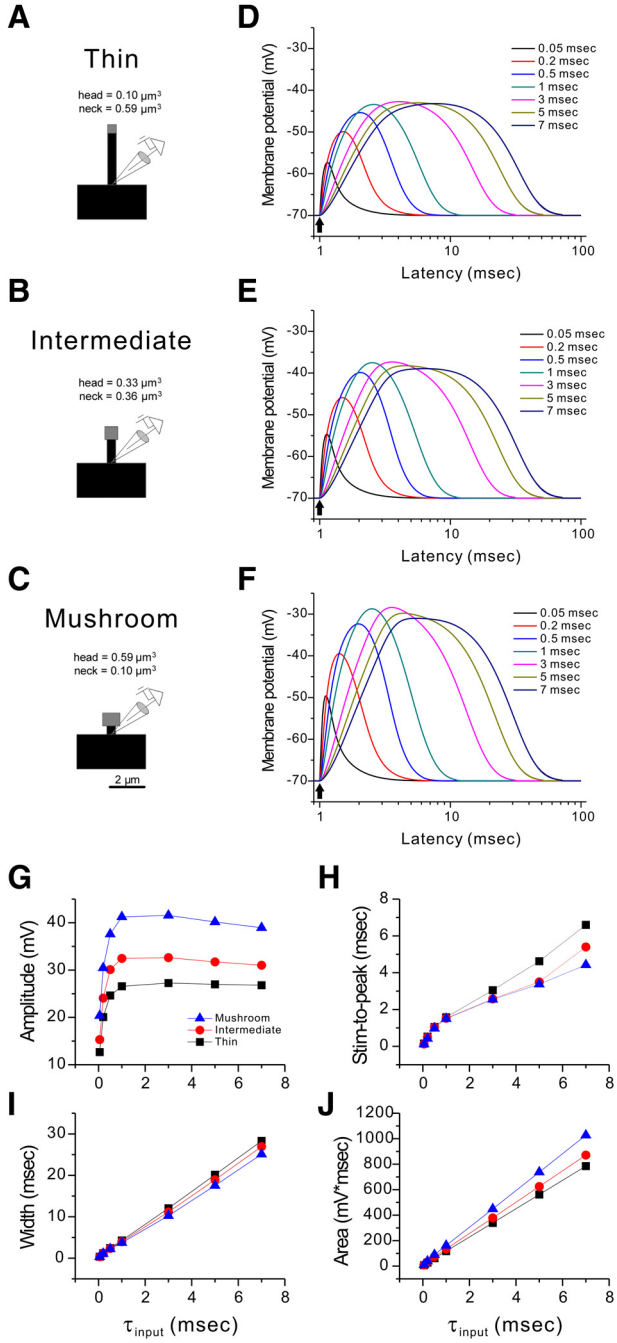

FIG. 5. Dendritic spine shapes were modeled based on the assumption that shape maturation occurs through the reorganization of the spine cytoskeleton. The volume of the spine remained constant, whereas the volumetric ratio of the spine neck and head changed to model a (*A*) thin spine, (*B*) intermediate spine, and (*C*) mushroom spine. Spines received excitatory synaptic conductance inputs on their head structure. Stimulation = black arrow. The resulting waveforms were graphed for (*D*) thin spines, (*E*) intermediate spines, and (*F*) mushroom spines. Graphs showing quantitative indices, such as peak amplitude (*G*), time-to-peak (*H*), width at 50% of peak (*I*), and area under curve (*J*), used to describe the EPSP for thin, intermediate, and mushroom spines, respectively.

through the mushroom spine than through the thin spine as the distance from the soma increased: up to an 8 and 11% increase for the thin and mushroom spines, respectively. These results demonstrate that spatial location affects the EPSP transduced through mushroom spines more than through thin spines.

Mushroom spines facilitate input summation

Presynaptic inputs may arrive on a single dendritic spine at different interstimulus latencies. The shape of the synaptic potential influences the temporal and spatial range at which potentials interact and summate. To investigate how inputs

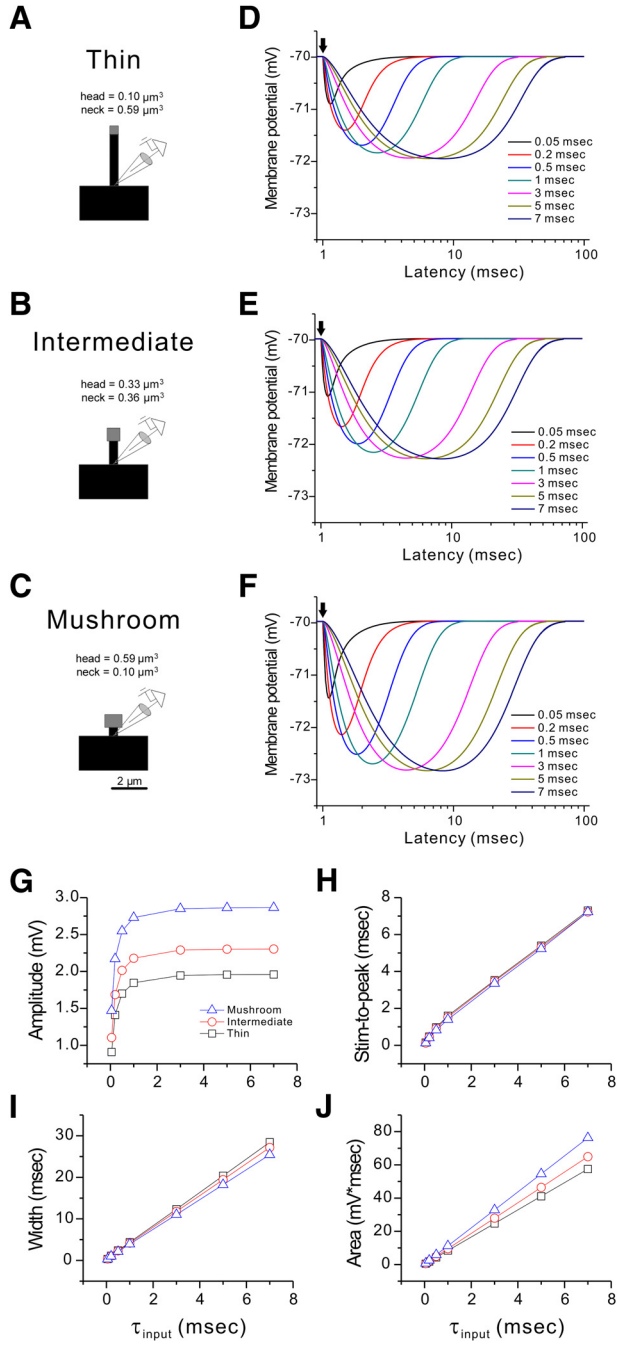

FIG. 6. Dendritic spine shapes were modeled based similar to the previous figure. The volume of the spine remained constant, whereas the volumetric ratio of the spine neck and head changed to model a (*A*) thin spine, (*B*) intermediate spine, and (*C*) mushroom spine. Spines received inhibitory synaptic conductance inputs on their head structure. Stimulation = black arrow. The resulting waveforms were graphed for (*D*) thin spines, (*E*) intermediate spines, and (*F*) mushroom spines. Graphs showing quantitative indices, such as peak amplitude (*G*), time-to-peak (*H*), width at 50% of peak (*I*), and area under curve (*J*), used to describe the IPSP for thin, intermediate, and mushroom spines, respectively.

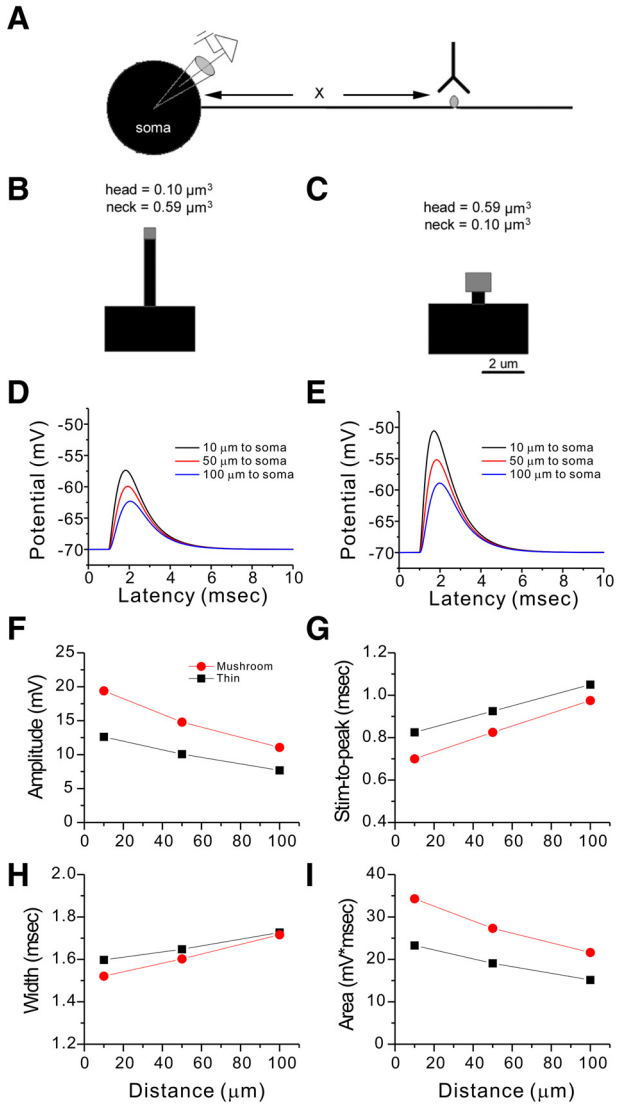

FIG. 7. Spine location affects the EPSP transduced through thin and mushroom-shaped spines. *A*: schematic of a simple neuron with either a thin or mushroom spine (gray oval) placed at variable distance (x) from the soma on the dendritic branch. Recordings were performed at the soma. *B*: thin or (*C*) mushroom spines with the same volume were modeled to transduce the excitatory synaptic conductance placed on the spine head. Initial input magnitude and duration remained constant. The resulting waveforms for (*D*) thin and (*E*) mushroom spines show that as distance from the soma increases, the amplitude decreases and the width of the EPSP increases. Graphs showing quantitative indices, such as peak amplitude (*G*), time-to-peak (*H*), width at 50% of peak (*I*), and area under curve (*J*), used to describe the EPSP for the thin and mushroom spine, respectively.

transduced through thin or mushroom spines influence input integration and somatic spiking, we constructed a simple neuronal model (Fig. 8*A*) (see METHODS). We placed a thin (Fig. 8*B*) or mushroom spine (Fig. 8*F*) on the dendrite 100 μm from the soma. We recorded evoked EPSPs from the base of the spine neck and soma. Because the amplitude of the response evoked by a given stimulus is different for thin and mushroom spines, we varied g_{max} to find somatic threshold: for thin spines g_{max} = 3.33 nS and mushroom spines g_{max} = 2.98 nS. These inputs on the thin spine (Fig. 8*C*) and the mushroom spine (Fig. 8*G*) produce subthreshold responses in the soma. Using these values, two excitatory inputs were given at different intervals. With an interstimulus interval of 9.69 ms EPSPs produced through both thin (Fig. 8*D*) and mushroom spines (Fig. 8*H*) summated sufficiently to activate an action potential in the soma. Increasing the latency between the two stimuli by 0.14 ms, to 9.83 ms, resulted in the failure of EPSPs to summate in the soma for the thin spine (Fig. 8*E*). In contrast, the inputs arriving through mushroom spines were still capable of summation and activated a spike in the soma (Fig. 8*I*). These data suggest that mature mushroom spines have characteristics that modify EPSPs, with properties that allow them to summate synaptic depolarizations more efficiently than thin spine shapes.

Spine shape limits effective interspine distance

The electrotonic distance between adjacent spines determines the extent of interaction between their propagated EPSPs. Because thin spines produce wider EPSPs than those produced by mushroom spines, with τ_{input} >3 ms (Fig. 5*I*), presynaptic inputs arriving through thin spines would be expected to interact with each other to a greater extent than similar inputs transduced through mushroom spines. To examine this phenomenon in our model, we placed two thin or

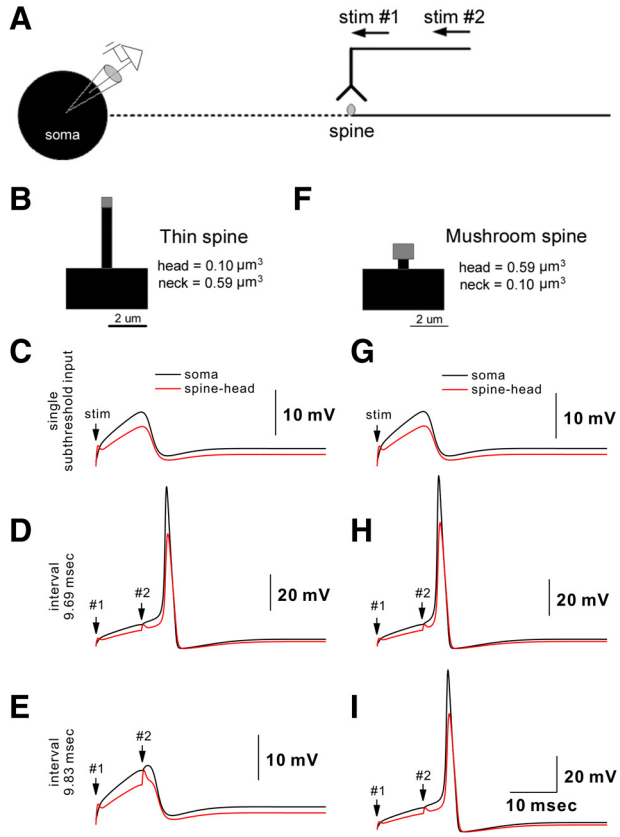

FIG. 8. Input integration occurs more efficiently through mushroom spines than through thin spines. *A*: schematic showing the modeled neuron with either a (*B*) thin or (*F*) mushroom spine attached to the dendritic branch. Recordings of the EPSP were performed at the soma and the base of the spine neck. Subthreshold excitatory stimulus on the spine head produced depolarizing synaptic potentials for both (*C*) thin and (*G*) mushroom spines. Two stimuli (#1 and #2) temporally separated by 9.69 ms summated sufficiently to activate a somatic action potential for (*D*) thin and (*H*) mushroom spines. *E*: increasing the interstimulus interval to 9.83 ms resulted in the failure of summation for synaptic potentials transduced through thin spines. *I*: inputs transmitted through mushroom spines resulted in summation and activation of a somatic action potential.

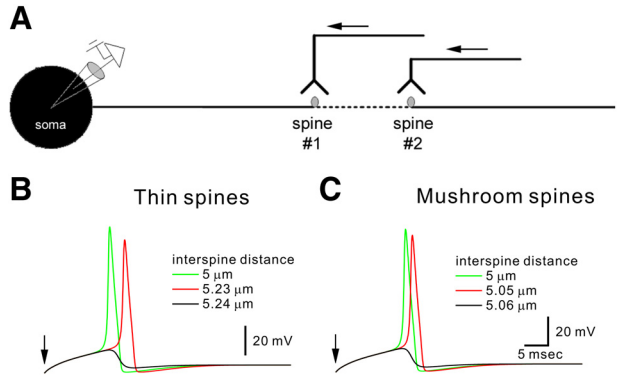

FIG. 9. Spine shape limits the effective interspine distance. *A*: a simple neuronal model was constructed with 2 thin or mushroom spines attached to the dendritic branch. The interspine distance varied, whereas 2 subthreshold stimuli were simultaneously activated on the spine. The resulting depolarization was recorded from the soma. When separated by 5 μm, the (*B*) 2 thin and (*C*) 2 mushroom spines produced EPSPs that summated and activated a somatic action potential. Summation failed for thin spines when the interspine distance exceeded 5.23 μm and failed for mushroom spines when the interspine distance exceeded 5.05 μm.

mushroom spines with dimensions shown in the previous figure on the dendritic branch (Fig. 9*A*) and calibrated the model such that the maximum conductance for a single spine was kept constant (τ_{input} = 3 ms, g_{max} = 0.28 nS) and produced a subthreshold EPSPs at the soma. The distal spine was located at a constant distance from the soma, whereas the location of the proximal spine varied such that the two spines had an interspine distance that varied from 5 to 5.24 μm. This interspine distance corresponds with an approximate spine density of 2.5 spines/5 μm dendritic branch, which is within the lower range of spine densities observed in vivo in the hippocampus (Garcia-Lopez et al. 2006). Within predefined parameters (see METHODS), when either the two thin (Fig. 9*B*) or two mushroom spines (Fig. 9*C*) were placed 5 μm away from each other, the presynaptic inputs summated sufficiently to activate an action potential in the soma. To determine the spatial interspine range at which two transduced synaptic potentials could interact for thin or mushroom spines, we progressively increased the interspine distance. Even with similar presynaptic input strength, the results show that thin spines had a larger interspine range than that of mushroom spines. Inputs transduced through two thin spines summated when the spines were separated from each other $\leq$5.23 μm. Increasing the interspine distance from 5.00 to 5.23 μm decreased the somatic action potential amplitude peak by 8.6 mV and increased the latency by 3.1 ms (Fig. 9*B*). At an interspine distance of 5.24 μm, the two inputs transmitted through the thin spines failed to summate effectively to activate a somatic action potential. Mushroom spines required a shorter interspine distance than that of thin spines for sufficient EPSP summation to produce an action potential. For an increase of interspine distance from 5.00 to 5.05 μm there was a 3.9-mV decrease in peak amplitude of the action potential and a slowing of latency to peak by 1.4 ms. Although the amplitude of individual EPSPs through each mushroom spine was greater, inputs failed to summate at an interspine distance of $>$5.05 μm. Subthreshold inputs on a pair of thin spines at an interspine distance of $\geq$5.05 summated and produced a somatic action potential (data not shown).

Mature mushroom-shaped spines confer neurons with improved frequency-following ability

Hyperexcitable DH neurons associated with neuropathic pain fire evoked and spontaneous action potentials at high frequencies and these signals must be propagated effectively through higher-order neurons associated with the pain-signaling pathway (Hains et al. 2003). Although the presence of inhibitory inputs and the kinetic properties of voltage-gated ion channels may modulate hyperexcitability, dendritic spines may also act as regulators of high-frequency excitatory activity. To examine the effects of spine shape on the frequency-following ability of the neuron, we used a similar simple neuronal model with two spines attached to the dendritic branch (Fig. 10*A*). The excitatory input on these spines was similar for both shapes, with the maximum conductance of 1.878 nS set to peak with τ_{input} = 0.2 ms. An excitatory conditioning stimulus was

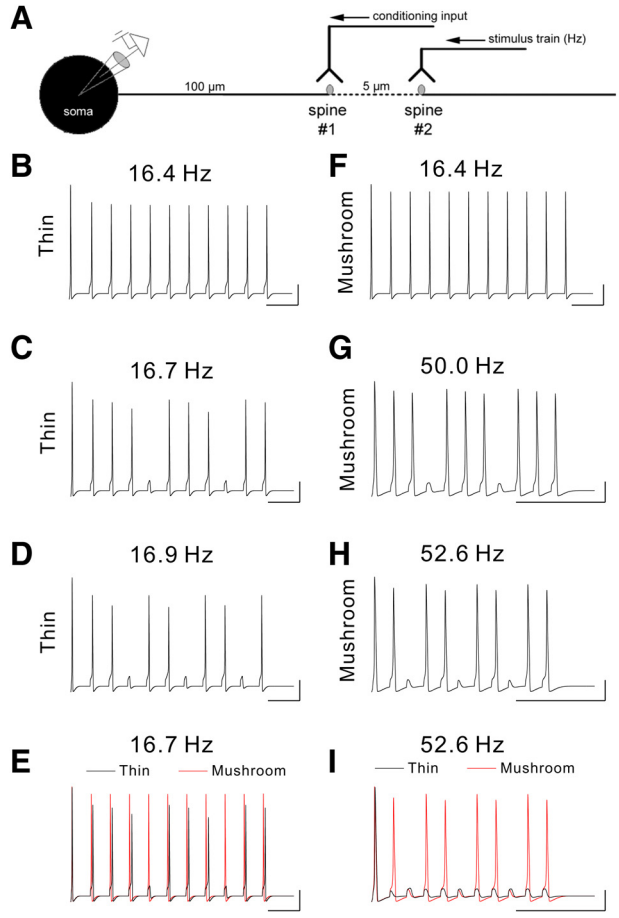

FIG. 10. Mushroom spine morphologies have better frequency-following ability than thin shaped spines. *A*: the simple neuron is similar to that shown in the previous figure. The distance of the proximal spine is 100 μm with the interspine distance of 5 μm. Following a conditioning AMPA-like excitatory stimulus on the proximal spine, the distal spine was subjected to a suprathreshold, AMPA-like excitatory stimulus train of varying frequencies. Thin (*B*) and mushroom (*F*) spines successfully propagated all stimuli equal to or slower than 16.4 Hz. *D*: thin spines successfully propagated 8 of 10 stimuli at 16.7 Hz. *E*: This rate of propagation progressively declined with 70% success at 16.9 Hz. *F*: At 16.7 Hz, mushroom spines (red line) propagated all inputs compared with thin spines (black line). *G*: mushroom spines propagated 8 of 10 stimuli at 50.0 Hz, nearly 3-fold the frequency of thin spines. *H*: at 52.6 Hz, the mushroom spines frequency-following abilities declined to 70% success. *I*: thin spines (black line) failed to propagate any inputs at this rate compared with mushroom spines (red line).

initiated on the proximal spine followed by a train of 10 stimuli at increasing frequencies on the distal spine. At 16.4 Hz, 10 somatic action potentials were produced in response to 10 test stimuli (100% success) in a dendrite with either thin or mushroom spines (Fig. 10, *B* and *F*). At 16.7 Hz, 8 somatic action potentials were produced in response to 10 test stimuli (80% success) in a dendrite with thin spines (Fig. 10*C*). A train of stimuli at 16.7 Hz on mushroom spines produced 10 of 10 somatic action potentials (100% success rate) (Fig. 10, *E* and *H*). Not until a much higher stimulus frequency of 50 Hz (Fig. 10*G*) did the success rate fall to 80% in a dendrite with mushroom spines. To reduce the success rate to 70%, the train of stimuli on thin spines needed to increase to only 16.9 Hz (Fig. 10*D*), whereas for mushroom spines, the success rate fell to 70% when the stimulus frequency increased to 52.6 Hz (Fig. 10*H*). For comparison, at 52.6 Hz, a dendrite with thin spines did not produce any successful somatic action potentials (Fig. 10*I*). These results demonstrate that a shift in the shape of the spine from one with a small head (thin spine) to a mushroom-shaped spine with a larger head structure confers a neuron with the ability to fire at higher frequency in response to repetitive stimulation. Thin spines can thus act as electrical low band-pass filters. As thin spines develop into mushroom spines, these structures would lose the ability to block high-frequency signals.

Mushroom spine shape reduces the effectiveness of inhibitory input

A loss of inhibitory inputs (i.e., decreased GABAergic innervation in the spinal cord after injury) (Drew et al. 2004; Hulsebosch et al. 2000) or a loss of the ability to transmit hyperpolarizing inputs could contribute to and maintain the increased excitability associated with central sensitization. The loss of inhibitory inputs can contribute to neuronal hyperexcitability after SCI. Inhibitory inputs onto spines located in proximity to the soma can block excitatory signals propagating from more distal locations along a dendrite (Nicoll et al. 1996). To test the effect of spine shape on the ability of inhibitory input to block transmission of excitatory potentials traveling toward the soma, an inhibitory GABA synapse was placed on the proximal thin or mushroom spine (Fig. 11*A*). Following a single inhibitory stimulus, the distal spine received a train of five suprathreshold excitatory stimuli at 37 Hz. Without activation of the inhibitory input, all five excitatory inputs produced somatic action potentials. With an inhibitory synaptic potential transduced through the thin spine, three of five excitatory inputs failed to generate somatic action potentials (Fig. 11*B*). In contrast, inhibition through a mushroom spine blocked two of five propagating excitatory potentials. This demonstrates that a change from a thin to a mushroom spine at proximal locations can significantly reduce the effectiveness of inhibitory inputs, which suggests a disinhibition mechanism underlying neuronal hyperexcitability associated with neuropathic pain.

Increasing the number of spines and altering spatial distribution can contribute to hyperexcitable neuronal output

Synaptic efficacy can increase in association with learning and memory or injury (Ji et al. 2003; Sandkuhler and Liu 1998; Stanton 1996) and is associated with the maturation of spine structure as well as increased dendritic spine density. The latter suggests that synaptic strength may increase through an increase in the number of inputs connected to the neuron. Previous data demonstrate that SCI induces an increase in DH neuron spine density, compared with that in DH neurons in intact spinal cords (an increase from 3.1 to 4 spines/10 μm dendrite), and redistributes spines closer to the soma (increase in spine density located 50 μm from the soma, 3 to 4.3 spines/10 μm dendrite) (Tan et al. 2008). Compared with intact animals (Fig. 1*C*), SCI resulted in increased spine density 1 mo after injury (Fig. 1*D*). To test the effects of these dendritic spine density/distribution changes, we modeled a simple neuron with spines distributed across a dendrite following a general distribution for spiny dorsal horn neurons in the spinal cord and cortical neurons (Garcia-Lopez et al. 2006; Ruiz-Marcos and Valverde 1969; Tan et al. 2008; Valverde and Ruiz-Marcos 1969) (see METHODS). This model is shown in Fig. 12*A* (*top*) and represents a DH neuron in a naïve spinal cord. Spines were evenly distributed over the dendritic branch, and all spines were constructed with thin-shaped morphology. Alternatively, evidence from the literature shows that the number and distribution of spines change after SCI (Kim et al. 2006). To test the effects of these post-SCI spine changes, we also constructed the simplified neuron model shown in Fig. 12*A* (*bottom*). The relative spine density and distribution for this model were obtained from previous morphological observations (Tan et al. 2008). To test both models, all spines were stimulated simultaneously. The threshold of simultaneous AMPA-like excitatory stimulation on all thin spines in the SCI neuron model (Fig. 12*B*, solid line) produced a single somatic action potential (g_{max} = 3.483 pS, τ_{input} = 0.2 ms), which was less than that for the intact neuron (g_{max} = 5.510 pS, τ_{input} = 0.2 ms). The latency and amplitude of action potential peak evoked by 5.510 pS were 7.6 ms and 24.3 mV for intact neurons and 2.2 ms and 38.2 mV for SCI neurons. Since there is also a switch in spine shape after SCI, we assumed the presence of mushroom spines that arise from the development of preexisting immature spines (Harris et al. 2003; Nishida and Okabe 2007; Yuste and Bonhoeffer 2001). To test the effect of

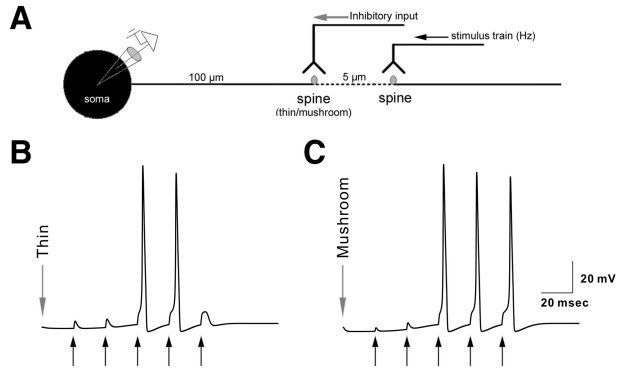

FIG. 11. Mushroom spines attenuate inhibitory input blockade of propagating excitatory potentials. *A*: schematic of neuronal model with a thin or mushroom proximal spine and a mushroom-shaped distal spine. The proximal spine was subjected to a GABA-like inhibitory stimulus followed by a train of 5 AMPA-like excitatory stimuli. This frequency of the stimulus train was kept constant. *B*: when the proximal spine was thin shaped, the inhibitory input (gray arrow) blocked 3 of 5 excitatory inputs. *C*: the inhibitory input transmitted through the mushroom-shaped spine blocked fewer, 2 of 5 excitatory inputs.

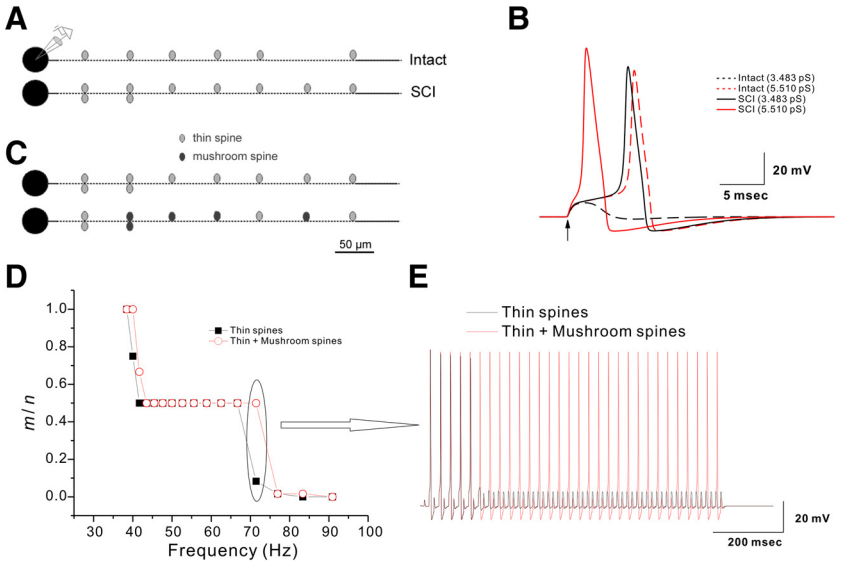

FIG. 12. Increased spine density and spine distribution after SCI can contribute to hyperexcitable neuronal output. *A*: a simple neuronal model was constructed based on anatomical data of deep spiny DH neurons. The data suggest that spine density increases and spine distribution shifts toward proximal dendritic location after SCI. As shown in *A* (*top*), the model for an intact neuron contains spines evenly distributed over a 350-μm length (*bottom*). After SCI, the number of dendritic spines increases and their density/distribution locates toward more proximal locations. *B*: the threshold of simultaneous AMPA-like excitatory stimulation on all thin spines for neuron model after SCI (solid line) to produce a single somatic action potential (g_{max} = 3.483 pS, τ_{input} = 0.2 ms) was less than that for the intact neuron (g_{max} = 5.510 pS, τ_{input} = 0.2 ms). *C*: next, we hypothesized that 5 thin spines were converted to mushroom spines in the SCI neuronal model. *D*: the response-to-stimulus ratio (*m*/*n*) is plotted as a function of the frequency. The SCI neuron model with 5 mushroom spines produces more action potentials at higher frequency. *E*: the representative action potentials were simulated at 71.4 Hz.

changing thin spines into mushroom-shaped spines, as is known to occur in vivo after SCI, five of the nine thin spines in the SCI neuron model were replaced with five spines with mushroom morphology (Fig. 12*C*, *top* and *bottom*). All spines in both models were simultaneously stimulated with a spike train of frequencies ranging from 38.5 to 90.9 Hz. The response-to-stimulus ratio (*m*/*n*) was plotted as a function of the frequency (Fig. 12*D*). The results show that the SCI neuron model containing mushroom spines continued to produce more action potentials at increasingly higher frequency. Importantly, there is a significant shift in the *n*:*m* ratio over a range of frequencies (~70–75 Hz), which corresponds to the range of elevated spike frequency observed in hyperexcitable WDR neurons in vivo post-SCI (Tan et al. 2008). As shown in Fig. 12*E*, when all spines were stimulated with a 71.4-Hz spike train, the intact neuron model containing thin spines only eventually failed to produce more than four action potentials, whereas the SCI neuron model continued to propagate action potentials at this high frequency. Taken together, the data demonstrate that the number and distribution of spines receiving excitatory input can contribute, along with dendritic spine shape, toward the production of neuronal hyperexcitability.

DISCUSSION

After injury to the spinal cord, spontaneous or evoked high-frequency firing in dorsal horn neurons is associated with neuropathic pain. Several factors are known to contribute to this injury-induced hyperexcitability: the loss of inhibitory inputs (Baba et al. 2003; Hains et al. 2002; Hulsebosch et al. 2000; Moore et al. 2002), inflammation (Hains and Waxman 2006; Hains et al. 2001; Ikeda et al. 2000; Woolf 1994), and changes in neuronal ion channel expression (Hains et al. 2003; Lampert et al. 2006; Waxman and Hains 2006). An additional contributor to neuropathic pain is the induction of spinal cord synaptic plasticity through processes that have been likened to mechanisms of learning and memory in the cortex (Ji et al. 2003; Sandkuhler and Liu 1998). Following injury, changes in postsynaptic dendritic spines may contribute to long-term maintenance of aberrant and strengthened synaptic connections. The unique geometric structure of spines affects the transduction of synaptic potentials and can alter the input–output function of neurons (Collin et al. 1997; Miller et al. 1985; Rall 1955; Rall et al. 1967, 1992; Rusakov et al. 1996; Segev and Rall 1988). The results we present here show that alteration in the morphology of dendritic spines after SCI can contribute to DH neuron hyperexcitablity, providing novel insights into mechanisms involved in neuropathic pain.

The primary question computational modeling can address is whether an underlying mechanism can account for the behavior of the system (Pongracz 1985). In this study, we incorporated morphological data on spine shape, size, and distribution, accrued in an investigation of DH neurons in spinal cord–injured rats (Tan et al. 2008) into a computational model based in NEURON. Results derived from the models we developed here should be viewed as qualitative rather than quantitative because of the limited experimental data available on dendritic spines on dorsal horn neurons. Our results, however, do provide a general idea of the biophysical events that arise after injury-induced dendritic spine changes. To examine the central question of whether changes in dendritic spine structure can contribute to DH neuron hyperexcitability associated with neuropathic pain we first began by simulating excitatory and inhibitory presynaptic inputs with previously described parameters (Destexhe et al. 1994; Pongracz 1985; Rall et al. 1967; Rusakov and Kullmann 1998). Although most dendritic spines receive excitatory glutamatergic synapses, some may have inhibitory properties (Calabrese et al. 2006). Because of this we modeled presynaptic inputs with kinetics similar to that of excitatory AMPA synapses (Fig. 2*A*, solid line) and inhibitory GABA synapses (Fig. 2*B*, dashed line) (Destexhe et al. 1994; Lopez-Aguado et al. 2002; Rusakov et al. 1996) and, as a comparison, we also tested other synaptic parameters on dendritic spine models.

The biophysical correlates of dendritic spine shapes and the influence on synaptic transmission and electrical transduction have been well studied (Segev and Rall 1988, 1998). The formation or maturation of spines from thin-shaped to mature, mushroom spines represents a shift toward more efficient and stronger synapses (Bourne and Harris 2007). The present results demonstrate that as the spine head size increases, the

amplitude of the synaptic potential increases, whereas the width of the waveform narrows. This phenomenon occurred for both EPSPs and IPSPs and for spines modeled on either of the two assumptions we used for their construction.

Our data show that spatially separated synaptic potentials are less likely to attenuate each other when transduced through mushroom spines, providing an isolation of presynaptic inputs, a property required for computations involving linear summation (Araya et al. 2006; Lev-Tov et al. 1983; Yuste and Urban 2004). This confers the dendrite with the ability to follow inputs arriving at higher frequency compared with thinner spines. An elaboration from thin to mushroom spines thus can increase high-frequency fidelity. As a consequence, however, mushroom spines contribute to hyperexcitability through signal amplification; increased fidelity of mushroom spines would reduce the ability of the neuron to filter high-frequency noise and increase the transmission of inputs from downstream hyperexcitable sources. Conversely, this suggests that thin spines act as low-pass filters for electrical inputs on a neuron. In our model, a switch from thin to mushroom spines increased frequency-following ability more than twofold; a similar increase to firing rates is observed after SCI in vivo (Hains et al. 2005; Tan et al. 2008).

The loss or reduction of inhibitory inputs on neurons in the dorsal horn contributes to hyperexcitability after SCI (Baba et al. 2003; Hains et al. 2002; Hulsebosch et al. 2000; Saruhashi et al. 1994; Tanabe et al. 2006). Anatomical evidence shows that inhibitory inputs arrive primarily at locations close to soma, which would allow these inputs to gate excessive activity (Nicoll et al. 1996). Our results show that inhibitory inputs arriving through thin spines are more effective than inputs arriving via mushroom spines in blocking propagating excitatory potentials. In addition to an increase in IPSPs amplitude and area, the IPSPs transduced through thin spines have a broader waveform, which can more readily interfere with propagating excitatory potentials. Therefore along with excitatory potentiation through a change in spine shape, a hyperexcitable input–output response can result from an attenuation of inhibitory gating as a result of the development of mushroom-shaped spines following SCI.

Changes in the density/distribution of dendritic spines have previously been shown in a number of experimental injury and disease models (Halpain et al. 2005; Kim et al. 2006; Stoltenburg-Didinger and Spohr 1983). Anatomical data on dorsal horn neurons suggest that following SCI there is an increase in dendritic spine density and distribution proximal to the soma in multireceptive DH neurons (Tan et al. 2008). The results presented here demonstrate that SCI-induced changes in spine density and distribution can increase the probability of excessive somatic spiking behavior. This occurs, in part, because of the larger and shorter postsynaptic depolarizations produced by inputs transmitted through mushroom spines compared with thin spines, especially when such spines are located closer to the soma (Fig. 7). The shorter depolarizing potentials of mushroom spines also suggested a narrowing of the absolute and relative refractory period (by reducing the number of ion channels entering the inactivated state), which would increase the availability of ion channels available for the next stimulation. Therefore a conversion of a percentage of thin spines into mushroom spines should allow the neuron to fire spikes at higher frequency. Interestingly, the SCI neuron model (containing mushroom spines) was able to spike consistently at >70 Hz, a frequency that fell within the range of frequencies observed in vivo for hyperexcitable neurons after contusion SCI (Tan et al. 2008). Our results demonstrate that dendritic spine changes can underlie changes in neuronal behavior that are observed in DH neurons and associated with pain after SCI.

In summary, these results implicate spatial and morphological remodeling of dendritic spines as a contributor to hyperexcitability of DH neurons associated with neuropathic pain after SCI. Our results suggest that by preventing or reversing injury-induced dendritic spine morphology, it may be possible to attenuate neuropathic pain.

GRANTS

This work was supported in part by grants from the Medical Research Service and Rehabilitation Research Service and Department of Veterans Affairs. The Center for Neuroscience and Regeneration Research is a collaboration of the Paralyzed Veterans of America and the United Spinal Association. B. C. Hains was funded by The American Pain Society and The Dana Foundation.

REFERENCES

Agrawal SK, Fehlings MG. Role of NMDA and non-NMDA ionotropic glutamate receptors in traumatic spinal cord axonal injury. *J Neurosci* 17: 1055–1063, 1997.

Araya R, Eisenthal KB, Yuste R. Dendritic spines linearize the summation of excitatory potentials. *Proc Natl Acad Sci USA* 103: 18799–18804, 2006.

Baba H, Ji RR, Kohno T, Moore KA, Ataka T, Wakai A, Okamoto M, Woolf CJ. Removal of GABAergic inhibition facilitates polysynaptic A fiber-mediated excitatory transmission to the superficial spinal dorsal horn. *Mol Cell Neurosci* 24: 818–830, 2003.

Bonhoeffer T, Yuste R. Spine motility: phenomenology, mechanisms, and function. *Neuron* 35: 1019–1027, 2002.

Bourne J, Harris KM. Do thin spines learn to be mushroom spines that remember? *Curr Opin Neurobiol* 17: 381–386, 2007.

Calabrese B, Wilson MS, Halpain S. Development and regulation of dendritic spine synapses. *Am J Physiol* 21: 38–47, 2006.

Carlisle HJ, Kennedy MB. Spine architecture and synaptic plasticity. *Trends Neurosci* 28: 182–187, 2005.

Chen LY, Rex CS, Casale MS, Gall CM, Lynch G. Changes in synaptic morphology accompany actin signaling during LTP. *J Neurosci* 27: 5363–5372, 2007.

Chetkovich DM, Chen L, Stocker TJ, Nicoll RA, Bredt DS. Phosphorylation of the postsynaptic density-95 (PSD-95)/discs large/zona occludens-1 binding site of stargazin regulates binding to PSD-95 and synaptic targeting of AMPA receptors. *J Neurosci* 22: 5791–5796, 2002.

Collin C, Miyaguchi K, Segal M. Dendritic spine density and LTP induction in cultured hippocampal slices. *J Neurophysiol* 77: 1614–1623, 1997.

Desmond NL, Levy WB. Synaptic interface surface area increases with long-term potentiation in the hippocampal dentate gyrus. *Brain Res* 453: 308–314, 1988.

Destexhe A, Mainen ZF, Sejnowski TJ. Synthesis of models for excitable membranes, synaptic transmission and neuromodulation using a common kinetic formalism. *J Comput Neurosci* 1: 195–230, 1994.

Drew GM, Siddall PJ, Duggan AW. Mechanical allodynia following contusion injury of the rat spinal cord is associated with loss of GABAergic inhibition in the dorsal horn. *Pain* 109: 379–388, 2004.

Finnerup NB, Johannesen IL, Fuglsang-Frederiksen A, Bach FW, Jensen TS. Sensory function in spinal cord injury patients with and without central pain. *Brain* 126: 57–70, 2003.

Finnerup NB, Johannesen IL, Sindrup SH, Bach FW, Jensen TS. Pain and dysesthesia in patients with spinal cord injury: a postal survey. *Spinal Cord* 39: 256–262, 2001.

Frank K, Fuortes MG. Unitary activity of spinal interneurones of cats. *J Physiol* 131: 424–435, 1956.

Galofre E, Ferrer I, Fabregues I, Lopez-Tejero D. Effects of prenatal ethanol exposure on dendritic spines of layer V pyramidal neurons in the somatosensory cortex of the rat. *J Neurol Sci* 81: 185–195, 1987.

Garcia-Lopez P, Garcia-Marin V, Freire M. Three-dimensional reconstruction and quantitative study of a pyramidal cell of a Cajal histological preparation. *J Neurosci* 26: 11249–11252, 2006.

Gazzaley A, Kay S, Benson DL. Dendritic spine plasticity in hippocampus. *Neuroscience* 111: 853–862, 2002.

Gruner JA. A monitored contusion model of spinal cord injury in the rat. *J Neurotrauma* 9: 123–128, 1992.

Hains BC, Everhart AW, Fullwood SD, Hulsebosch CE. Changes in serotonin, serotonin transporter expression and serotonin denervation supersensitivity: involvement in chronic central pain after spinal hemisection in the rat. *Exp Neurol* 175: 347–362, 2002.

Hains BC, Klein JP, Saab CY, Craner MJ, Black JA, Waxman SG. Upregulation of sodium channel Nav1.3 and functional involvement in neuronal hyperexcitability associated with central neuropathic pain after spinal cord injury. *J Neurosci* 23: 8881–8892, 2003.

Hains BC, Saab CY, Waxman SG. Changes in electrophysiological properties and sodium channel Nav1.3 expression in thalamic neurons after spinal cord injury. *Brain* 128: 2359–2371, 2005.

Hains BC, Waxman SG. Activated microglia contribute to the maintenance of chronic pain after spinal cord injury. *J Neurosci* 26: 4308–4317, 2006.

Hains BC, Yucra JA, Hulsebosch CE. Reduction of pathological and behavioral deficits following spinal cord contusion injury with the selective cyclooxygenase-2 inhibitor NS-398. *J Neurotrauma* 18: 409–423, 2001.

Halpain S. They're plastic, but they recycle. *Neuron* 52: 746–748, 2006.

Halpain S, Spencer K, Graber S. Dynamics and pathology of dendritic spines. *Prog Brain Res* 147: 29–37, 2005.

Harris KM, Fiala JC, Ostroff L. Structural changes at dendritic spine synapses during long-term potentiation. *Philos Trans R Soc Lond B Biol Sci* 358: 745–748, 2003.

Harris KM, Kater SB. Dendritic spines: cellular specializations imparting both stability and flexibility to synaptic function. *Annu Rev Neurosci* 17: 341–371, 1994.

Hodgkin AL, Huxley AF. A quantitative description of membrane current and its application to conduction and excitation in nerve. *J Physiol* 117: 500–544, 1952.

Hulsebosch CE, Xu GY, Perez-Polo JR, Westlund KN, Taylor CP, McAdoo DJ. Rodent model of chronic central pain after spinal cord contusion injury and effects of gabapentin. *J Neurotrauma* 17: 1205–1217, 2000.

Ikeda H, Asai T, Murase K. Robust changes of afferent-induced excitation in the rat spinal dorsal horn after conditioning high-frequency stimulation. *J Neurophysiol* 83: 2412–2420, 2000.

Ji RR, Kohno T, Moore KA, Woolf CJ. Central sensitization and LTP: do pain and memory share similar mechanisms? *Trends Neurosci* 26: 696–705, 2003.

Kim BG, Dai HN, McAtee M, Vicini S, Bregman BS. Remodeling of synaptic structures in the motor cortex following spinal cord injury. *Exp Neurol* 198: 401–415, 2006.

Lampert A, Hains BC, Waxman SG. Upregulation of persistent and ramp sodium current in dorsal horn neurons after spinal cord injury. *Exp Brain Res* 174: 660–666, 2006.

Lev-Tov A, Miller JP, Burke RE, Rall W. Factors that control amplitude of EPSPs in dendritic neurons. *J Neurophysiol* 50: 399–412, 1983.

Lopez-Aguado L, Ibarz JM, Varona P, Herreras O. Structural inhomogeneities differentially modulate action currents and population spikes initiated in the axon or dendrites. *J Neurophysiol* 88: 2809–2820, 2002.

Matsuzaki M. Factors critical for the plasticity of dendritic spines and memory storage. *Neurosci Res* 57: 1–9, 2007.

Matsuzaki M, Honkura N, Ellis-Davies GC, Kasai H. Structural basis of long-term potentiation in single dendritic spines. *Nature* 429: 761–766, 2004.

Miller JP, Rall W, Rinzel J. Synaptic amplification by active membrane in dendritic spines. *Brain Res* 325: 325–330, 1985.

Moore KA, Kohno T, Karchewski LA, Scholz J, Baba H, Woolf CJ. Partial peripheral nerve injury promotes a selective loss of GABAergic inhibition in the superficial dorsal horn of the spinal cord. *J Neurosci* 22: 6724–6731, 2002.

Nakayama AY, Harms MB, Luo L. Small GTPases Rac and Rho in the maintenance of dendritic spines and branches in hippocampal pyramidal neurons. *J Neurosci* 20: 5329–5338, 2000.

Nicoll A, Kim HG, Connors BW. Laminar origins of inhibitory synaptic inputs to pyramidal neurons of the rat neocortex. *J Physiol* 497: 109–117, 1996.

Nishida H, Okabe S. Direct astrocytic contacts regulate local maturation of dendritic spines. *J Neurosci* 27: 331–340, 2007.

Park M, Salgado JM, Ostroff L, Helton TD, Robinson CG, Harris KM, Ehlers MD. Plasticity-induced growth of dendritic spines by exocytic trafficking from recycling endosomes. *Neuron* 52: 817–830, 2006.

Pongracz F. The function of dendritic spines: a theoretical study. *Neuroscience* 15: 933–946, 1985.

Rall W. A statistical theory of monosynaptic input–output relations. *J Cell Physiol* 46: 373–411, 1955.

Rall W. Distinguishing theoretical synaptic potentials computed for different soma-dendritic distributions of synaptic input. *J Neurophysiol* 30: 1138–1168, 1967.

Rall W, Burke RE, Holmes WR, Jack JJ, Redman SJ, Segev I. Matching dendritic neuron models to experimental data. *Physiol Rev* 72: S159–S186, 1992.

Rall W, Burke RE, Smith TG, Nelson PG, Frank K. Dendritic location of synapses and possible mechanisms for the monosynaptic EPSP in motoneurons. *J Neurophysiol* 30: 1169–1193, 1967.

Romero MI, Rangappa N, Li L, Lightfoot E, Garry MG, Smith GM. Extensive sprouting of sensory afferents and hyperalgesia induced by conditional expression of nerve growth factor in the adult spinal cord. *J Neurosci* 20: 4435–4445, 2000.

Ruiz-Marcos A, Valverde F. The temporal evolution of the distribution of dendritic spines in the visual cortex of normal and dark raised mice. *Exp Brain Res* 8: 284–294, 1969.

Rusakov DA, Kullmann DM. Extrasynaptic glutamate diffusion in the hippocampus: ultrastructural constraints, uptake, and receptor activation. *J Neurosci* 18: 3158–3170, 1998.

Rusakov DA, Stewart MG, Korogod SM. Branching of active dendritic spines as a mechanism for controlling synaptic efficacy. *Neuroscience* 75: 315–323, 1996.

Sandkuhler J, Liu X. Induction of long-term potentiation at spinal synapses by noxious stimulation or nerve injury. *Eur J Neurosci* 10: 2476–2480, 1998.

Saruhashi Y, Young W, Hassan AZ, Park R. Excitatory and inhibitory effects of serotonin on spinal axons. *Neuroscience* 61: 645–653, 1994.

Segev I, Rall W. Computational study of an excitable dendritic spine. *J Neurophysiol* 60: 499–523, 1988.

Segev I, Rall W. Excitable dendrites and spines: earlier theoretical insights elucidate recent direct observations. *Trends Neurosci* 21: 453–460, 1998.

South SM, Kohno T, Kaspar BK, Hegarty D, Vissel B, Drake CT, Ohata M, Jenab S, Sailer AW, Malkmus S, Masuyama T, Horner P, Bogulavsky J, Gage FH, Yaksh TL, Woolf CJ, Heinemann SF, Inturrisi CE. A conditional deletion of the NR1 subunit of the NMDA receptor in adult spinal cord dorsal horn reduces NMDA currents and injury-induced pain. *J Neurosci* 23: 5031–5040, 2003.

Stanton PK. LTD, LTP, and the sliding threshold for long-term synaptic plasticity. *Hippocampus* 6: 35–42, 1996.

Stoltenburg-Didinger G, Spohr HL. Fetal alcohol syndrome and mental retardation: spine distribution of pyramidal cells in prenatal alcohol-exposed rat cerebral cortex; a Golgi study. *Brain Res* 313: 119–123, 1983.

Svendsen F, Tjolsen A, Gjerstad J, Hole K. Long term potentiation of single WDR neurons in spinalized rats. *Brain Res* 816: 487–492, 1999.

Tan AM, Stamboulian S, Chang YW, Zhao P, Hains AB, Waxman SG, Hains BC. Neuropathic pain memory is maintained by Rac1-regulated dendritic spine remodeling after spinal cord injury. *J Neurosci* 28: 13173–13183, 2008.

Tanabe M, Murakami H, Honda M, Ono H. Gabapentin depresses C-fiber-evoked field potentials in rat spinal dorsal horn only after induction of long-term potentiation. *Exp Neurol* 202: 280–286, 2006.

Tashiro A, Minden A, Yuste R. Regulation of dendritic spine morphology by the rho family of small GTPases: antagonistic roles of Rac and Rho. *Cereb Cortex* 10: 927–938, 2000.

Tashiro A, Yuste R. Regulation of dendritic spine motility and stability by Rac1 and Rho kinase: evidence for two forms of spine motility. *Mol Cell Neurosci* 26: 429–440, 2004.

Tsay D, Yuste R. Role of dendritic spines in action potential backpropagation: a numerical simulation study. *J Neurophysiol* 88: 2834–2845, 2002.

Tsay D, Yuste R. On the electrical function of dendritic spines. *Trends Neurosci* 27: 77–83, 2004.

Valverde F, Ruiz-Marcos A. Dendritic spines in the visual cortex of the mouse: introduction to a mathematical model. *Exp Brain Res* 8: 269–283, 1969.

Waxman SG, Hains BC. Fire and phantoms after spinal cord injury: Na(+) channels and central pain. *Trends Neurosci* 29: 207–215, 2006.

Wiens KM, Lin H, Liao D. Rac1 induces the clustering of AMPA receptors during spinogenesis. *J Neurosci* 25: 10627–10636, 2005.

Wilson CJ. Passive cable properties of dendritic spines and spiny neurons. *J Neurosci* 4: 281–297, 1984.

Woolf CJ. A new strategy for the treatment of inflammatory pain. Prevention or elimination of central sensitization. *Drugs* 47, *Suppl*. 5: 1–9; discussion: 46–47, 1994.

Woolf CJ, Shortland P, Coggeshall RE. Peripheral nerve injury triggers central sprouting of myelinated afferents. *Nature* 355: 75–78, 1992.

Yuste R, Bonhoeffer T. Morphological changes in dendritic spines associated with long-term synaptic plasticity. *Annu Rev Neurosci* 24: 1071–1089, 2001.

Yuste R, Majewska A. On the function of dendritic spines. *Neuroscientist* 7: 387–395, 2001.

Yuste R, Urban R. Dendritic spines and linear networks. *J Physiol* (*Paris*) 98: 479–486, 2004.